Development of High-Bandgap AlGaInP Solar Cells Grown by Organometallic Vapor-Phase Epitaxy

Emmett E. Perl, John Simon, John F. Geisz, Waldo Olavarria, Michelle Young, Anna Duda, Daniel J. Friedman, and Myles A. Steiner

***Abstract*—AlGaInP solar cells with bandgaps between 1.9 and 2.2 eV are investigated for use in next-generation multijunction photovoltaic devices. This quaternary alloy is of great importance to the development of III–V solar cells with five or more junctions and for cells optimized for operation at elevated temperatures because of the high bandgaps required in these designs. In this work, we explore the conditions for the organometallic vapor-phase epitaxy growth of AlGaInP and study their effects on cell performance. Initial efforts focused on developing ∼2.0-eV AlGaInP solar cells with a nominal aluminum composition of 12%. Under the direct spectrum at 1000 W/m^2 (AM1.5D), the best of these samples had an open-circuit voltage of 1.59 V, a bandgap-voltage offset of 440 mV, a fill factor of 88.0%, and an efficiency of 14.8%. We then varied the aluminum composition of the alloy from 0% to 24% and were able to tune the bandgap of the AlGaInP layers from ∼1.9 to ∼2.2 eV. While the samples with a higher aluminum composition exhibited a reduced quantum efficiency and increased bandgap-voltage offset, the bandgap-voltage offset remained at 500 mV or less, up to a bandgap of ∼2.1 eV.**

***Index Terms*—Photovoltaic cells, semiconductor epitaxial layers, solar energy, III–V semiconductor materials.**

I. Introduction

MULTIJUNCTION solar cells have long achieved the highest efficiencies of any photovoltaic technology. Today, the world's best devices consist of four or more III–V semiconductor junctions and have attained power conversion efficiencies greater than 38% at 1 sun and 45% under concentration [1]. To achieve these high efficiencies, each of the subcells needs to meet a few key requirements. First, they must have a bandgap (E_g) that is close to optimal in order to minimize the combined thermalization and nonabsorption loss in the final structure [2]–[5]. Second, they must be composed of excellent quality materials with effective passivation layers in order to avoid substantial losses to the open-circuit voltage ($V_{\rm OC}$) and short-circuit current density ($J_{\rm SC}$). Today's best four-junction devices have demonstrated a bandgap-voltage offset ($W_{\rm OC} = E_g/q - V_{\rm OC}$) $\leq$ 400 mV for each subcell when illuminated at 1 sun, which is indicative of the excellent material quality of these devices [6], [7]. Third, for operation in a two-terminal series-connected configuration, the cell integration requires proper optical design and the development of a tunnel junction interconnect [2]. Even though lattice-matching constraints make it difficult to grow each subcell on the same substrate, the most efficient multijunction solar cells reported to date have been successfully integrated into monolithic two-terminal devices using either semiconductor bonding or lattice-mismatched growth techniques [6]–[8].

While four-junction photovoltaic devices have attained great success in recent years, the field is rapidly moving toward designs with five or six semiconductor junctions to further increase efficiencies [8], [9]. While the ternary alloy GaInP can be grown lattice-matched to GaAs with excellent material quality and a near-optimal bandgap for a four-junction device [10], high-quality top cells with larger bandgap energies are desired for five-junction and six-junction photovoltaic devices [4], [5]. Higher bandgaps are also preferred for photovoltaic devices that are operated at elevated temperatures. Landis *et al*. reported on the development of high-temperature solar cells for near-sun space missions and showed how the optimal room-temperature (RT) bandgap of a single-junction solar cell shifts from ∼1.4 eV for operation at 25 °C to ∼2.3 eV for operation at 900 °C [11].

We are interested in developing a two-junction photovoltaic device that can operate efficiently at temperatures up to 400 °C for use in photovoltaic thermal hybrid solar collectors [12]. Fig. 1 shows the modeled efficiency of a two-junction device as a function of operating temperature and the RT bandgap of the top cell. This model constrains the RT bandgap of the bottom subcell to 1.42 eV (GaAs) and assumes a concentration of 1000 suns, a 1-sun $W_{\rm OC}$ of 400 mV for each subcell at RT and that all absorbed photons are converted into photocurrent. The key takeaway from this plot is that the ideal RT bandgap of the top cell increases and that the cell efficiency decreases as the operating temperature is increased. A two-junction device with RT subcell bandgaps of 2.0 and 1.42 eV is nearly optimal when operated at 400 °C and can theoretically reach an efficiency greater than 25%.

The quaternary alloy AlGaInP offers the highest direct bandgap of any III–V material that is lattice-matched to GaAs. It is, therefore, a promising candidate for use in five-junction and six-junction photovoltaic devices, as well as for solar

Manuscript received October 27, 2015; revised February 2, 2016; accepted February 23, 2016. Date of publication March 29, 2016; date of current version April 19, 2016. This work was supported by the U.S. Department of Energy under Contract DE-AC36-08GO28308 with the National Renewable Energy Laboratory and funded in part by the ARPA-E FOCUS program under Award DE-AR0000508. The U.S. Government retains and the publisher, by accepting the article for publication, acknowledges that the U.S. Government retains a nonexclusive, paid-up, irrevocable, worldwide license to publish or reproduce the published form of this work, or allow others to do so, for U.S. Government purposes.

E. E. Perl is with the National Renewable Energy Laboratory, CO 80401 USA, and also with the Department of Electrical and Computer Engineering, University of California at Santa Barbara, Santa Barbara, CA 93106 USA (e-mail: emmett.perl@nrel.gov).

J. Simon, J. F. Geisz, W. Olavarria, M. Young, A. Duda, D. J. Friedman, and M. A. Steiner are with the National Renewable Energy Laboratory, CO 80401 USA (e-mail: john.simon@nrel.gov; john.geisz@nrel.gov; waldo.olavarria@nrel.gov; michelle.young@nrel.gov; anna.duda@nrel.gov; daniel.friedman@nrel.gov; myles.steiner@nrel.gov).

Color versions of one or more of the figures in this paper are available online at http://ieeexplore.ieee.org.

Digital Object Identifier 10.1109/JPHOTOV.2016.2537543

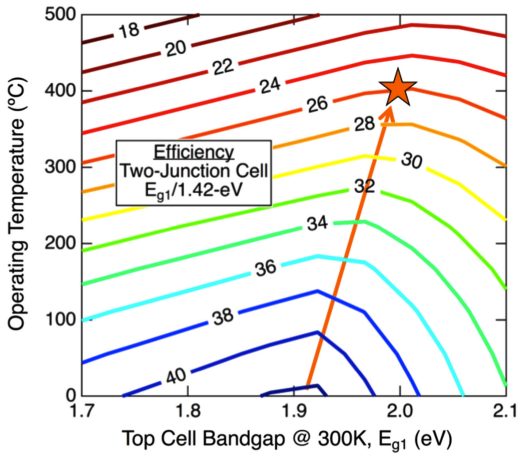

Fig. 1. Modeled efficiency of a two-junction photovoltaic device as a function of the top-cell RT (300 K) bandgap and the operating temperature.

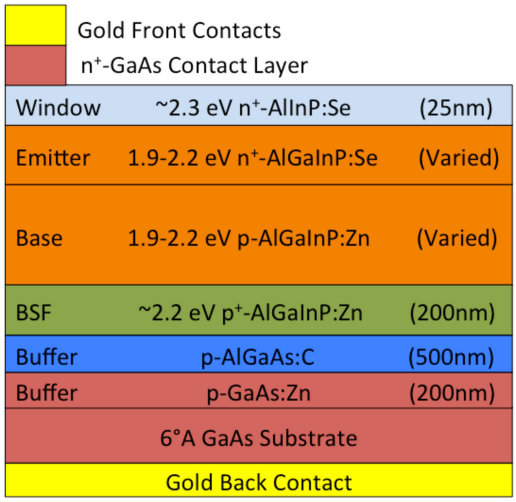

Fig. 2. Schematic showing the structure of the epitaxially grown layers and metallization of the AlGaInP solar cells studied in this paper. The diagram is not to scale.

cells operated at high temperature. By varying the aluminum content of the alloy and controlling the CuPt-ordering in the group III sublattice, direct bandgaps between approximately 1.8 and 2.2 eV are achievable [13], [14].

While AlGaInP has great potential for improving the efficiency of the next generation of multijunction devices, there are several technical challenges that accompany its development. Chief among these is the issue of oxygen contamination, which can be problematic for any aluminum-containing material due to the high dissociation energy of the bond between aluminum and oxygen [14]–[18]. The incorporation of oxygen is often associated with the formation of deep-level traps that can greatly increase the nonradiative recombination rate of a material [19], [20].

Despite the growth challenges, a number of groups have worked to develop high-bandgap AlGaInP cells [21]–[24]. Masuda *et al*. reported an upright 2.0-eV AlGaInP subcell grown by molecular beam epitaxy with a $W_{\rm OC}$ of 620 mV but with a significantly lower internal quantum efficiency (IQE) than a GaInP cell [21]. Hongbo *et al.* demonstrated an upright 2.05-eV AlGaInP subcell grown by organometallic vapor-phase epitaxy (OMVPE) with a $W_{\rm OC}$ of 595 mV but observed degradation in the IQE as well [22]. Cornfeld *et al.* developed an inverted 2.05-eV AlGaInP solar cell grown by OMVPE that achieved a $W_{\rm OC}$ of 510 mV with less degradation in the IQE [23]. Recently, Wanlass *et al.* reported an upright 1.95-eV AlGaInP cell with a $W_{\rm OC}$ of 485 mV and minimal IQE loss [24]. Even with these significant advances in cell performance, no AlGaInP cell reported to date has achieved comparable performance with that of the best GaInP subcells of the same configuration [10]. Reducing the $W_{\rm OC}$ while maintaining a high IQE is the key to successfully integrating AlGaInP into a multijunction device.

In this work, we demonstrate a ∼2.0-eV AlGaInP solar cell with a $W_{\rm OC}$ of 440 mV and minimal degradation to the IQE compared with upright GaInP solar cells grown under the same conditions. We reported preliminary work on the development of ∼2.0-eV AlGaInP solar cells in [25] and studied the impact of substrate miscut, emitter dopant species, and growth temperature (T_g) on cell performance. Here, we include three new significant results. First, we report additional details on the growth conditions of our ∼2.0-eV AlGaInP solar cells, including studies showing the importance of having a high growth rate (R_g) and phosphine partial pressure. Second, we show how the thickness of the emitter and base affect carrier collection in the device. Third, we study the impact of aluminum composition on cell performance by growing devices with bandgaps ranging from 1.9 to 2.2 eV.

II. Experimental Methods

All the samples in this study were grown using an atmospheric-pressure OMVPE vertical reactor. The reactor is custom-built and uses trimethylgallium (TMGa), triethylgallium (TEGa), trimethylindium (TMIn), trimethylaluminum (TMAl), arsine (AsH_3), and phosphine (PH_3) sources. Diethylzinc (DEZn) was added to p-dope the back-surface field (BSF) and base layers, and dilute hydrogen selenide (H_2Se/H_2) was added to n-dope the emitter and window layers. The samples were grown on zinc-doped (0 0 1) GaAs substrates miscut 6° toward <111>A. Prior to growth, the substrates were etched for 1 min in a NH_4OH:H_2O_2:H_2O (2:1:10) solution. The graphite susceptor at the center of the reactor was heated to a temperature of 1000 °C to drive excess oxygen out of the reactor before the substrate was loaded.

Fig. 2 shows a schematic of the device that includes the nominal bandgap and thickness of the semiconductor layers. A ∼500-nm $Al_{0.3}Ga_{0.7}As$ buffer layer was grown prior to the active device layers in order to getter residual oxygen early in the growth. The AlGaInP BSF has a nominal aluminum composition of 27%, and the AlInP window layer has a nominal aluminum composition of 53%. With the exception of the samples from Section III-C, the nominal emitter and base thicknesses are 90 and 900 nm, respectively. With the exception of the samples from Section III-D, the nominal aluminum composition in the AlGaInP emitter and base is 12%, corresponding to a bandgap of ∼2.0 eV. Unless otherwise noted, the active layers were grown

TABLE I
SOLAR CELL PARAMETERS FOR SAMPLES GROWN AT DIFFERENT TEMPERATURES

Sample	T_g (°C)	Strain (%)	E_g (eV)	V_{OC} (V)	W_{OC} (mV)	J_{SC} (mA/cm^2)	FF (%)	Efficiency (%)
MN742	700	0.026	1.99	1.49	500	10.9	73.1	11.9
MN746	720	0.028	2.00	1.51	490	10.6	81.7	13.0
MN750	740	0.036	2.01	1.55	460	10.7	87.9	14.6
MN753	760	0.043	2.02	1.56	460	10.7	88.4	14.7
MN775	780	0.076	2.03	1.59	440	10.6	88.0	14.8
MN779	800	0.142	2.05	1.57	480	10.3	88.2	14.2

Efficiencies are quoted for the direct spectrum at 1000 W/m^2.

at a temperature of 740 °C, a rate of ∼6.5 μm/h, and a phosphine flow of ∼200 sccm. The 2.0-eV samples grown with varying T_g were antireflection coated using a bilayer of ZnS/MgF_2.

After the AlGaInP cells were processed, we measured their external quantum efficiency (EQE) and reflectance (R) using a custom-built test setup. The IQE can be calculated using the following equation:

$$\mathrm{IQE}(\lambda) = \frac{\mathrm{EQE}(\lambda)}{1 - \mathrm{R}(\lambda)}. \quad (1)$$

The bandgap of the active layers was determined by subtracting *kT*/2 from the peak emission energy measured by RT electroluminescence (EL) [26], [27]. It is important to note that this resulted in a bandgap and W_{OC} that is ∼20 mV higher than what we previously determined using EQE measurements [25]. The aluminum compositions were estimated by calculating the molar flow rates of the group-III precursors. RT Hall and capacitance–voltage measurements were taken to estimate the concentrations of the n-type and p-type dopants in the AlGaInP emitter and base. We took illuminated current–voltage (LIV) and dark current–voltage (DIV) measurements using a custom-built solar simulator that uses a Xenon lamp and adjustable high-brightness LEDs. The spectrum and intensity were adjusted using calibrated reference cells to simulate the AM1.5D spectrum at 1000 W/m^2. These test setups are discussed in more detail elsewhere [2], [6], [12].

III. RESULTS AND DISCUSSION

A. Growth Temperature

The material quality of OMVPE-grown AlGaInP is very sensitive to T_g, which affects both oxygen incorporation and CuPt-type ordering [13]–[16], [28]. To study the impact of T_g on cell performance, we grew a set of ∼2.0-eV solar cells where we varied the T_g of the AlGaInP layers from 700 °C to 800 °C, while keeping all other growth conditions the same.

Table I shows the measured cell parameters for each of these devices. We found that cell performance improved as the T_g was increased up to 780 °C. By increasing T_g from 700 °C to 780 °C, we were able to decrease the W_{OC} from 500 to 440 mV, increase the fill factor from 73.1% to 88.0%, and increase the efficiency from 11.9% to 14.8%. Fig. 3 shows the DIV characteristics for each of these cells. The dashed lines indicate the slopes of ideal diodes with ideality factors of 1 and 2, where the *y*-intercepts are equal to J_{01} for the $n = 1$ line and J_{02} for the $n = 2$ line. It is clear that both J_{01} and J_{02} decrease as the T_g was increased up to 780 °C. These reduced dark currents correlate to higher V_{OC}s and are indicative of lower nonradiative recombination rates in the emitter and base.

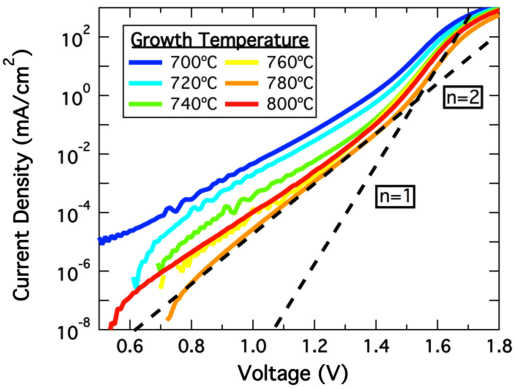

Fig. 3. DIV characteristics of AlGaInP solar cells grown at temperatures ranging from 700 °C to 800 °C.

We attempted to measure oxygen concentrations by secondary ion mass spectrometry, but the levels were near the instrument detection limit of ∼10^{17} cm^{-3}, and therefore, the measurement did not give a reliable indication of the oxygen variation. However, the improvement in performance at high T_g is consistent with a reduction in oxygen incorporation. It is well known that high growth temperatures can suppress the incorporation of oxygen due to the increased probability of desorption from the surface [14], [15]. Minimizing oxygen incorporation can help reduce the nonradiative recombination rate in the AlGaInP layers, which can significantly improve cell performance [14], [17], [18].

There are a number of other important trends that we observed. First, we found that the bandgap increases with T_g. This can be partially explained by a decrease in CuPt-type ordering with growth temperature [13], [14], [29]. However, the higher bandgaps could also be a result of lower indium incorporation at high T_g. Using an *in-situ* wafer curvature measurement technique (MOS) [30], we observed increased tensile strain as the T_g was increased. This is quantified in Table I. The particularly high strain for the sample grown at 800 °C could explain why its performance started to degrade.

It is also important to stress that none of the OMVPE flow rates were changed as the T_g was varied. This resulted in lower concentrations of the zinc and selenium dopants for the samples

TABLE II
SOLAR CELL PARAMETERS FOR SAMPLES GROWN AT 780 °C WITH VARYING EMITTER AND BASE DOPING CONCENTRATIONS

Sample	N_A (cm^{-3})	N_D (cm^{-3})	V_{OC} (V)	J_{SC}, AM1.5D (mA/cm^2)
MN904	5.5×10^{16}	8.7×10^{17}	1.56	7.5
MN908	6.3×10^{16}	1.8×10^{18}	1.56	7.3
MN912	6.0×10^{16}	3.0×10^{18}	1.55	6.9
MN989	2.9×10^{16}	8.1×10^{17}	1.58	7.7
MN991	5.7×10^{16}	7.9×10^{17}	1.58	7.7
MN993	7.0×10^{16}	8.3×10^{17}	1.57	7.6

grown at high temperatures because, like oxygen, both zinc and selenium incorporate less efficiently at high T_g [16]. Specifically, as T_g was raised from 740 °C to 780 °C, we measured a decrease in the emitter doping (N_D) from 1.1×10^{18} to 8.7×10^{17} cm^{-3} and a decrease in the base doping (N_A) from 1.2×10^{17} to 5.6×10^{16} cm^{-3}. This change in the doping concentration could also have a significant impact on the cell performance [31]–[33]. For this reason, we ran an experiment where we varied the emitter and base doping flows for six solar cells grown at 780 °C. The results of this study are summarized in Table II.

The H_2Se/H_2 flow rates for MN904, MN908, and MN912 were 2.5, 5, and 10 sccm, respectively. The DeZn flow rates for MN989, MN991, and MN993 were 5, 10, and 20 sccm, respectively. First, note that the measured doping concentrations do not scale in the same proportions as the dopant flow rates, suggesting that the incorporation of zinc and selenium saturate at relatively low concentrations. Second, we observed a decrease in the IQE as the emitter doping was increased. This is what we would expect since increased doping will lead to an increase in the number of impurities that act as recombination centers for minority carriers, resulting in a reduced minority carrier diffusion length in the n-type emitter [34], [35]. Finally, we observed a change of only ~10 mV in the V_{OC} as the doping concentrations were varied in these studies. This suggests that the material quality is improving at high T_g and that the increased performance cannot be explained by the change in doping concentration alone.

B. Growth Rate and Phosphine Partial Pressure

The R_g and phosphine partial pressure may also have a strong influence on the incorporation of oxygen in aluminum-containing alloys because they affect the surface kinetics during growth. As the R_g is increased, the exposure time of the surface decreases, and therefore, oxygen atoms have less time to adsorb and accumulate before the surface layer is buried. As the phosphine partial pressure is increased, there will be additional group V elements to compete with oxygen for surface adsorption sites, helping to suppress the incorporation of oxygen [14]. Note that our atmospheric-pressure OMVPE reactor allows us to achieve higher partial pressures than a low-pressure reactor.

To study the impact of the R_g and phosphine partial pressure on cell performance, we grew two sets of devices. For the first set, we varied the phosphine flow in the AlGaInP layers from 50 to 200 sccm while keeping the R_g constant at 6 μm/h. For the second set, we varied the R_g of the AlGaInP layers from 2 to 6 μm/h while keeping the phosphine flow constant at 200 sccm.

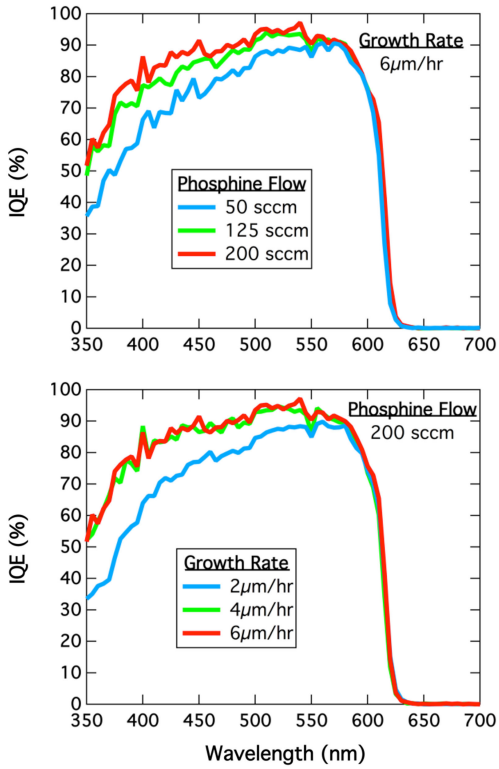

Fig. 4. Wavelength-dependent IQE of ~2.0-eV AlGaInP solar cells with (top) varying phosphine flow and (bottom) varying growth rate.

The IQEs of these samples are shown in Fig. 4. As the phosphine flow was increased from 50 to 200 sccm, there was a clear improvement in the short-wavelength IQE that can be attributed to an increase in the minority carrier diffusion length in the n-type emitter. This is consistent with a lower oxygen concentration in the AlGaInP layers, which has been shown to decrease as the phosphine overpressure is increased [14], [17], [18]. However, we also observed a reduction in the doping concentration in the emitter from 3.0×10^{18} to 1.2×10^{18} cm^{-3} as the phosphine flow was increased from 50 to 200 sccm. This lower doping would also result in a longer diffusion length in the emitter, which could lead to a higher IQE. The base doping remained around 10^{17} cm^{-3}, and the V_{OC} varied by less than 10 mV for all three samples.

As the R_g was increased from 2 to 4 μm/h, there was a notable improvement in the IQE and a ~30-mV increase in the V_{OC}. As the R_g was further increased to 6 μm/h, we saw almost no change in the IQE but measured a ~10-mV increase in the V_{OC}. There was a negligible difference in the emitter and base doping concentrations for these three samples. These trends are consistent with previous studies on how the R_g and phosphine partial pressure impact oxygen incorporation in aluminum-containing III–V materials [14], [17], [18].

C. Thickness of the Emitter and Base

Nearly all investigations of AlGaInP and AlGaAs solar cells have observed a significantly shorter minority carrier diffusion

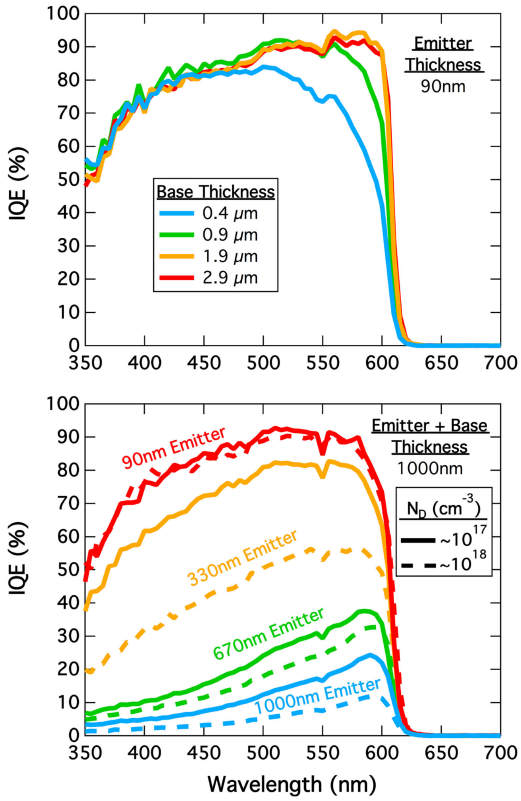

Fig. 5. Wavelength-dependent IQE of ∼2.0-eV AlGaInP solar cells with (top) varying base thickness and (bottom) varying emitter thickness. In the bottom graph, the doping concentration in the emitter (N_D) was either 10_{17} (solid lines) or 10^{18} cm^{-3} (dashed lines).

length in the n-type emitter than in the p-type base [8], [19], [21]–[23]. This typically manifests itself in a substantial reduction in the short-wavelength IQE of the device, which leads to a loss of photocurrent and can have a dramatic impact on current matching in a multijunction solar cell. By optimizing the OMVPE growth conditions, we were able to minimize this IQE loss in our ∼2.0-eV front-junction AlGaInP solar cells. However, there is still a significant difference between the minority carrier diffusion length of the n-type emitter and the p-type base in these devices.

Fig. 5 shows how the IQE was impacted as the emitter and base thicknesses were varied. As we increased the base thickness from 0.4 to 1.9 μm, there was a clear improvement in the long-wavelength IQE. This is because the cells with a 0.4- and 0.9-μm base are not optically thick and absorb only a fraction of the long-wavelength light. We observed minimal change in the IQE as the base thickness was further increased from 1.9 to 2.9 μm. Both of these devices retained an IQE >90% near the band edge, suggesting that these cells are close to optically thick and are collecting most of the carriers generated far from the junction. This is indicative of the long diffusion length in the p-type base.

As the n-type emitter thickness was increased, we observed a dramatic reduction in the short-wavelength IQE. For this set of samples, we kept the total thickness of the emitter and base constant at 1 μm. For this reason, the reduction in the IQE is not a result of a changing absorption thickness and can instead be attributed to a difference in the minority carrier diffusion length of the n-type emitter and p-type base.

Since the doping concentration can have a notable impact on the diffusion length of a material, we grew an additional set of samples where the doping concentration in the n-type emitter (N_D) was lowered from $\sim 10^{18}$ to $\sim 10^{17}$ cm^{-3}. While this resulted in a consistent improvement in the IQE, we still observed a dramatic reduction in the IQE as the emitter thickness was increased. These results show the significant difference in the collection efficiency between n-type and p-type AlGaInP and suggest that improvements to the material quality of n-type AlGaInP could be a key driver to attaining high efficiency in a five-junction or six-junction solar cell. Furthermore, these results are in stark contrast with recent reports of rear heterojunction GaInP solar cells with thick low-doped n-type emitters, which have maintained a high IQE while achieving the highest V_{OC} and efficiency of any GaInP solar cell reported to date [10].

D. Aluminum Composition

In order to integrate an AlGaInP subcell into a five-junction or six-junction photovoltaic device, it is important to be able to tune the bandgap of the top cell to attain the highest possible V_{OC} while remaining current matched to the lower subcells. One straightforward way to raise the bandgap and V_{OC} of an AlGaInP solar cell is to increase the aluminum composition of the alloy. However, it is well documented that alloys with higher aluminum content are more susceptible to oxygen incorporation [14], [17]–[19], [21]–[23]. To study the impact of aluminum composition on cell performance, we grew a set of samples where we varied the nominal aluminum composition in the emitter and base from 0% to 24%, although no further optimization was done for each sample.

Fig. 6 shows the IQE and LIV characteristics for each of these devices. The bandgaps derived from EL measurements range from 1.90 eV for AlGaInP with a 0% nominal aluminum composition to 2.17 eV for AlGaInP with a 24% nominal aluminum composition. This corresponds to a bandgap increase of ∼11 meV per 1% increase in the aluminum fraction. We measured <8% reduction in the peak IQE as the nominal aluminum composition was raised from 0% to 18%. However, we observed a much more significant drop in the IQE as the aluminum composition was further increased to 24%. Further analysis is required to understand the precise origin of the degradation, but the trends are consistent with both an increase in oxygen incorporation as the aluminum fraction is raised and with a less-effective passivation as the barrier heights for the window layer and BSF are reduced. The abrupt drop in performance for the 24% aluminum-containing sample could also be related to the direct/indirect crossover for lattice-matched AlGaInP, which occurs at an aluminum composition of ∼27%. Similar trends have been observed for AlGaInP LEDs [14].

The LIV measurements from Fig. 6 give some indication as to how these cells would perform when integrated into a multijunction device. Increasing the material bandgap means that the

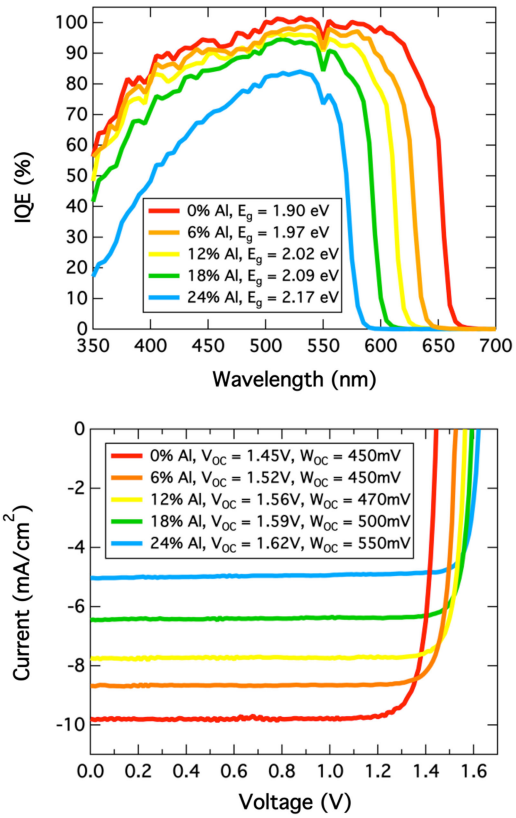

Fig. 6. (Top) IQE and (bottom) LIV characteristics of AlGaInP solar cells grown with nominal aluminum compositions ranging from 0% to 24%.

active layers are going to absorb less light, which corresponds to a decrease in the J_{SC}. Increasing the bandgap will also lead to a reduction in thermalization loss, resulting in a higher V_{OC}. However, we also saw an increase in the W_{OC} as the aluminum composition was raised, which is what we would expect if oxygen contamination was becoming more problematic as aluminum is added to the alloy. Despite this degradation, the W_{OC} remained at 500 mV or less up to a bandgap of ~2.1 eV, which is our target top cell bandgap for future five-junction and six-junction photovoltaic devices. By further optimizing the growth conditions at this bandgap, we expect to demonstrate even better cell performance.

IV. Conclusion

We have developed high-bandgap AlGaInP solar cells grown by OMVPE for use in next-generation multijunction photovoltaic devices. Increasing the growth temperature from 700 °C to 780 °C for ~2.0-eV AlGaInP devices led to a decrease in the W_{OC} from 500 to 440 mV and an increase in the efficiency from 11.9% to 14.8%. We found that growing at a high growth rate and phosphine partial pressure is important to maintaining a high IQE. By varying the junction position and cell thickness, we found that the minority carrier diffusion length in the n-type emitter is significantly shorter than the p-type base, suggesting that the thickness of each of these layers is critical to the cell design. We then grew samples with bandgaps ranging from 1.90 to 2.17 eV by varying the aluminum composition in the alloy and found that the material quality degraded as the aluminum composition was increased. Despite this degradation, we maintained a W_{OC} of 500 mV or less up to a bandgap of 2.1 eV. These devices exceed the performance of the best AlGaInP solar cells reported to date, which is an important step toward integrating AlGaInP subcells into multijunction photovoltaic devices with five or more junctions and into dual-junction cells designed for high-temperature operation.

Acknowledgment

The authors are grateful for very helpful discussions with Minjoo Larry Lee, Clay McPheeters, Paul Sharps, Daehwan Jung, and Joseph Faucher.

References

[1] M. A. Green, K. Emery, Y. Hishikawa, W. Warta, and E. D. Dunlop, "Solar cell efficiency tables (version 45)," *Prog. Photovoltaics, Res. Appl.*, vol. 23, no. 1, pp. 1–9, 2015.

[2] D. J. Friedman, J. M. Olson, and S. R. Kurtz, "High-efficiency III-V multijunction solar cells," in *Handbook of Photovoltaic Science and Engineering*, 2nd ed., A. Luque and S. Hegedus, Eds. Chichester, U.K.: Wiley, 2011, pp. 314–364.

[3] W. Shockley and H. J. Queisser, "Detailed balance limit of efficiency of p-n junction solar cells," *J. Appl. Phys.*, vol. 32, no. 3, pp. 510–519, 1961.

[4] D. C. Law *et al.*, "Future technology pathways of terrestrial III-V multijunction solar cells for concentrator photovoltaic systems," *Sol. Energy Mater. Sol. Cells*, vol. 94, no. 8, pp. 1314–1318, 2010.

[5] R. R. King *et al.*, "Band-gap-engineered architectures for high-efficiency multijunction concentrator solar cells," in *Proc. 24th Eur. Photovoltaic Sol. Energy Conf. Exhib.*, 2009, pp. 55–61.

[6] R. M. France *et al.*, "Quadruple junction inverted metamorphic concentrator devices," *IEEE J. Photovoltaics*, vol. 5, no. 1, pp. 432–437, Jan. 2015.

[7] F. Dimroth *et al.*, "Wafer bonded four-junction GaInP/GaAs//GaInAsP/GaInAs concentrator solar cells with 44.7% efficiency," *Prog. Photovoltaics, Res. Appl.*, vol. 22, no. 3, pp. 277–282, 2014.

[8] P. T. Chiu *et al.*, "Direct semiconductor bonded 5J cell for space and terrestrial applications," *IEEE J. Photovoltaics*, vol. 4, no. 1, pp. 493–497, Jan. 2014.

[9] P. Patel *et al.*, "Initial results of the monolithically grown six-junction inverted metamorphic multi-junction solar cell," in *Proc 38th IEEE Photovoltaic Spec. Conf.*, 2012, pp. 1–4.

[10] J. F. Geisz, M. A. Steiner, I. Garcia, S. R. Kurtz, and D. J. Friedman, "Enhanced external radiative efficiency for 20.8% efficient single-junction GaInP solar cells," *Appl. Phys. Lett.*, vol. 103, no. 4,, art. no. 041118, 2013.

[11] G. A. Landis, D. Merritt, R. Raffaelle, and D. Scheiman, "High-temperature solar cell development," in *Proc. 18th Space Photovoltaic Res. Technol. Conf.*, 2005, pp. 241–247.

[12] H. M. Branz, W. Regan, K. Gerst, J. B. Borak, and E. A. Santori, "Hybrid solar converters for maximum exergy and inexpensive dispachable energy," *Energy Environ. Sci.*, vol. 8, no. 11, pp. 3083–3091, 2015.

[13] A. Mascarenhas, Ed. *Spontaneous Ordering in Semiconductor Alloys*. Norwell, MA, USA: Kluwer, 2002, pp. 8–20.

[14] G. B. Stringfellow and M. G. Craford, Eds., *High Brightness Light Emitting Diodes, Semiconductors and Semimetals*, vol. 48. New York, NY, USA: Academic, 1997, pp. 97–148.

[15] M. Kondo *et al.*, "Origin of nonradiative recombination centers in AlGaInP grown by metalorganic vapor phase epitaxy," *J. Electron. Mater.*, vol. 23, no. 3, pp. 355–358, 1994.

[16] M. Kondo *et al.*, "Crystallographic orientation dependence of impurity incorporation into III-V compound semiconductors grown by metalorganic vapor phase epitaxy," *J. Appl. Phys.*, vol. 76, no. 2, pp. 914–927, 1994.

[17] G. B. Stringfellow, *Organometallic Vapor-Phase Epitaxy: Theory and Practice*. New York, NY, USA: Academic, 1999, pp. 427–433.

[18] S. A. Stockman *et al.*, "Oxygen incorporation in AlInP, and its effect on p-type doping with magnesium," *J. Electron. Mater.*, vol. 28, no. 7, pp. 916–925, 1999.

[19] S. Heckelmann, D. Lackner, C. Karcher, F. Dimroth, and A. W. Bett, "Investigations on AlGaAs solar cells grown by MOVPE," *IEEE J. Photovoltaics*, vol. 5, no. 1, pp. 446–453, Jan. 2015.
[20] S. Nojima, H. Tanaka, and H. Asahi, "Deep electron trapping center in Si-doped InGaAlP grown by molecular-beam epitaxy," *J. Appl. Phys.*, vol. 59, no. 10, pp. 3489–3494, 1986.
[21] T. Masuda, S. Tomasulo, J. R. Lang, and M. L. Lee, "Comparison of single junction AlGaInP and GaInP solar cells grown by molecular beam epitaxy," *J. Appl. Phys.*, vol. 117, no. 9, art. no. 094504, 2015.
[22] L. Hongbo *et al.*, "A 2.05 eV AlGaInP sub-cell used in next generation solar cells," *J. Semicond.*, vol. 35, no. 9, art. no. 094010, 2014.
[23] A. B. Cornfeld, P. Patel, J. Spann, D. Aiken, and J. McCarty, "Evolution of a 2.05 eV AlGaInP top sub-cell for 5 and 6J-IMM applications," in *Proc 38th IEEE Photovoltaic Spec. Conf.*, 2012, pp. 002788–002791.
[24] M. W. Wanlass *et al.*, "Progress toward an advanced four-subcell inverted metamorphic multi-junction (IMM) solar cell," *Prog. Photovoltaics, Res. Appl.*, vol. 24, no. 2, pp. 139–149, 2016.
[25] E. E. Perl *et al.*, "Development of a 2.0 eV AlGaInP solar cell grown by OMVPE," in *Proc. 42nd IEEE Photovoltaic Spec. Conf.*, 2015, pp. 1–6.
[26] M. A. Steiner *et al.*, "Effects of internal luminescence and internal optics on Voc and Jsc of III-V solar cells," *IEEE J. Photovoltaics*, vol. 3, no. 4, pp. 1437–1442, Oct. 2013.
[27] J. I. Pankove, *Optical Processes in Semiconductors*. North Chelmsford, MA, USA: Courier, 2012.
[28] A. Le Donne *et al.*, "Optical and electrical characterization of AlGaInP solar cells," *Sol. Energy Mater. Sol. Cells*, vol. 94, no. 12, pp. 2002–2006, 2010.
[29] L. C. Su, I. H. Ho, and G. B. Stringfellow, "Control of ordering in Ga0.5In0.5P using growth temperature," *J. Appl. Phys.*, vol. 76, no. 6, pp. 3520–3525, 1994.
[30] R. M. France *et al.*, "Lattice-mismatched 0.7-eV GaInAs solar cells grown on GaAs using GaInP compositionally graded buffers," *IEEE J. Photovoltaics*, vol. 4, no. 1, pp. 190–195, Jan. 2014.
[31] S. R. Kurtz *et al.*, "Passivation of interfaces in high-efficiency photovoltaic devices," *MRS Proc.*, vol. 573, p. 95, 1999.
[32] H. J. Hovel, "Solar cells," in *Semiconductors and Semimetals*, vol. 11, R. K. Willardson and A. C. Beer, Eds. New York, NY, USA: Academic, 1975.
[33] A. L. Fahrenbruch and R. H. Bube, *Fundamentals of Solar Cells*. New York, NY, USA: Academic, 1983 pp. 69–104.
[34] G. B. Lush *et al.*, "A study of minority carrier lifetime versus doping concentration in n-type GaAs grown by metalorganic chemical vapor deposition," *J. Appl. Phys.*, vol. 72, no. 4, pp. 1436–1442, 1992.
[35] M. P. Lumb, M. A. Steiner, J. F. Geisz, and R. J. Walters, "Incorporating photon recycling into the analytical drift-diffusion model of high efficiency solar cells," *J. Appl. Phys.*, vol. 116, no. 19, art. no. 194504, 2014.

Authors' photographs and biographies not available at the time of publication.